Submitted to the International Europhysics Conference on High Energy Physics,
EPS97, Jerusalem, Israel, August 1997

Determination of the Strong Coupling Constant from Integrated Jet Rates in Deep Inelastic Scattering

H1 Collaboration

Abstract:

A determination of the strong coupling constant $\alpha_s(M_Z^2)$ is presented. Jet rates in deep inelastic ep-scattering at HERA are evaluated following the strategy described in a previous H1 publication. Using most recent, improved next to leading order calculations and the JADE jet algorithm $\alpha_s(Q^2)$ values are extracted in four different bins of the negative squared momentum transfer Q^2 in the range from 40 GeV^2 to 4000 GeV^2. A combined fit of these several $\alpha_s(Q^2)$ determinations to the renormalization group equation results in $\alpha_s(M_Z^2) = 0.115 \pm 0.003\,(stat)\,^{+0.008}_{-0.011}\,(sys) + 0.006\,(reco.\ scheme)$. The analysis uses on data samples which correspond to integrated luminosities of 6.57 pb^{-1} taken with the H1 detector in 1994 and 1995 for $Q^2 > 100$ GeV^2 and of 2.74 pb^{-1} taken in 1994 for $Q^2 < 100$ GeV^2.

Abstract 246
Parallel Sessions 2,3,4
Plenary Sessions 1,3,4

1 Introduction

The hadronic final state in neutral current deep inelastic electron proton scattering (DIS) at HERA can be used to test QCD as in e^+e^- collider experiments, and the strong coupling constant $\alpha_s(M_Z^2)$ can be determined. M_Z is the mass of the neutral vector boson. For it the multi-jet production is studied using data taken with the H1 detector at the HERA ep-collider at DESY.

The basic DIS-reaction can be written as $e + p \to e' + X$, where X denotes an arbitrary hadronic final state. The process is sketched in figure 1, in which the four-momentum vectors of the particles are given in brackets to define the used kinematic quantities later in the text.

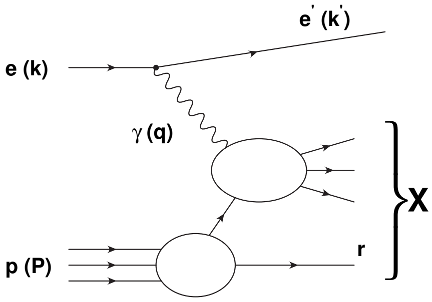

Figure 1: A sketch of neutral current deep inelastic ep-scattering.

To lowest order, neutral current DIS jet production can be described as purely electromagnetic scattering of the electron off a quark via single photon exchange[1]. This scattering leads to (1+1) jet events. One jet is caused by the scattered quark (1), the other by the proton remnant r (+1), which is only partially observed in the H1 detector.

Higher jet multiplicities are described in the framework of QCD. The corresponding cross sections are expressed as power series in the strong coupling constant α_s, such that the leading order (LO) contribution to (2+1) jet events is of $\mathcal{O}(\alpha_s)$. Two generic graphs contribute (see figure 2), where the hard subprocess is either gluon or quark induced. As both diagrams contain couplings to gluons it is clear that (2+1) jet production is sensitive to α_s.

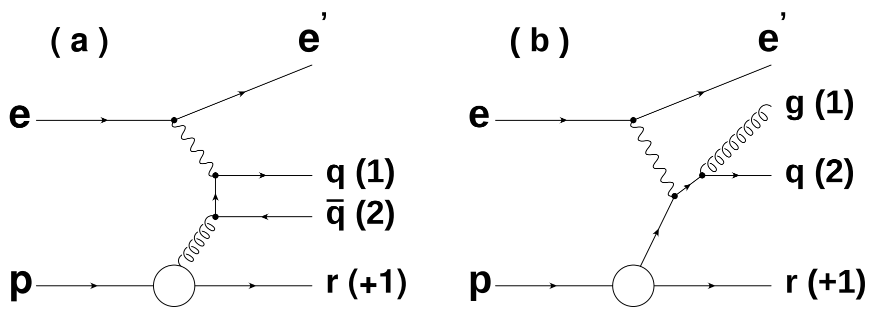

Figure 2: Generic Feynman diagrams of the LO contributions to (2+1) jet events.

The analysis presented in this paper essentially follows the strategy of the previous α_s determination [1], but relies on a most recent next to leading order (NLO) QCD-calculation. In

[1] In the Q^2 range under study ($Q^2 < 4000$ GeV^2 with the present statistics) effects due to the exchange of the intermediate vector boson $Z°$ are smaller than 3% and are negligible.

the theoretical calculation used in [1] terms proportional to the product of the squared invariant mass of the hadronic final state $W^2 = (q + P)^2$ and the JADE jet resolution parameter were neglected. Therefore these calculations were not valid for large values of W^2, especially in the region of low $Q^2 = -q^2 = -(k - k')^2$, the negative four momentum transfer squared between the in- and outgoing electron. Also no recombination scheme was defined in this NLO calculation in order to combine partons to jets. In the improved NLO calculations available now no terms are neglected, different recombination schemes are defined as in the experimental treatment, and several jet algorithms are implemented.

In order to extract α_s measured (2+1) jet rates at the detector level are corrected to the parton level. Comparing these jet rates in different bins of Q^2 to a NLO QCD-prediction $\alpha_s(Q^2)$ values are extracted over a wide range of Q^2. The independent $\alpha_s(Q^2)$ values are then used to determine $\alpha_s(M_Z^2)$ by performing a fit to the renormalization group equation as discussed in [1]. The use of an improved NLO QCD-calculation program allows an estimation of the dependence of $\alpha_s(M_Z^2)$ on different recombination schemes. The analysis is performed by determining the (2+1) jet rate using the JADE jet algorithm, for which a lot of experience has been gathered in recent years.

The data used were taken with the H1 detector at HERA in 1994 and correspond to an integrated luminosity of 2.74 pb^{-1}. For $Q^2 > 100$ GeV^2 in addition an integrated luminosity of 3.83 pb^{-1} taken in the year 1995 is used. The HERA collider was operated with positrons of 27.5 GeV momentum and protons of 820 GeV momentum leading to a center of mass energy $\sqrt{s}$ of about 300 GeV.

2 H1 apparatus

A detailed discussion of the H1 apparatus can be found elsewhere [10]. Here emphasis is put on describing the main features of the components of the detector relevant to this analysis, which makes use mainly of the calorimeters and, to a lesser extent, of the central and backward tracking systems. The polar angle, θ, is defined with respect to the proton beam direction, which is identified with the $+z$-axis.

The inner part of the detector consists of the central tracking chamber supplemented by a forward tracking detector and a backward proportional chamber (BPC), covering the polar angle ranges $25° < \theta < 155°$, $7° < \theta < 25°$ and $155° < \theta < 175°$, respectively. The central and forward tracking devices are used to determine the vertex position. The central tracking chamber and the BPC, together with the vertex, are used to measure the electron scattering angle in the central and backward region. The angular resolution achieved is better than 1 mrad.

The energy of the scattered electron is measured in a liquid argon (LAr) calorimeter and in a backward electromagnetic lead-scintillator calorimeter (BEMC); the LAr calorimeter is also used for a measurement of the hadronic energy flow. The solenoid is outside the LAr calorimeter and provides a uniform magnetic field of 1.15 T parallel to the proton beam axis throughout the tracking region.

The LAr calorimeter [11] extends over the polar angle range $4° < \theta < 153°$ with full azimuthal coverage. The scattered electron enters the LAr for events in which Q^2 is larger than about 100 GeV^2. The calorimeter consists of an electromagnetic section with lead absorbers, corresponding to a depth of between 20 and 30 radiation lengths, and a hadronic section with steel absorbers. The total depth of the LAr calorimeter varies between 4.5 and 8 hadronic interaction lengths. Test beam measurements of LAr calorimeter modules have demonstrated energy resolutions of $\sigma(E)/E \approx 0.12/\sqrt{E/\,\mathrm{GeV}} \oplus 0.01$ for electrons [12] and $\sigma(E)/E \approx 0.5/\sqrt{E/\,\mathrm{GeV}} \oplus 0.02$ for charged pions [14]. The uncertainty of the absolute energy scale for electrons is at the level of 2%. The hadronic energy scale has been verified from the balance of transverse momentum between hadronic jets and the scattered electron in DIS events and is known to a precision of 4%.

The BEMC, with a thickness of 22.5 radiation lengths, covers the backward region of the detector, $151^\circ < \theta < 177^\circ$. It is mainly used to trigger on and to measure electrons from DIS processes at low Q^2. The acceptance region corresponds to Q^2 values in the approximate range $5 \leq Q^2 \leq 100$ GeV^2. A resolution of $\sigma(E)/E \approx 0.10/\sqrt{E/\,\mathrm{GeV}} \oplus 0.03$ has been achieved. By adjusting the measured electron energy spectrum to the kinematic peak the BEMC energy scale is known to an accuracy of 1%. Since 1995 the BEMC and BPC in the backward region have been replaced by a lead/scintillating fibre calorimeter (SPACAL) and a drift chamber (BDC). Hence for $Q^2 < 100$ GeV^2 only data taken in 1994 are used in the analysis presented here.

3 Event Selection

The data are divided into two sub-samples according to the detector construction. The sub-samples consist of DIS events with the scattered electron detected and well contained in the BEMC or in the LAr calorimeter. The selection criteria follow closely those of the F_2^p analysis using the 1994 data [13].

Events in the first sub-sample (BEMC) must satisfy the following requirements:

1. The four-momentum transfer Q^2 must be between 10 and 100 GeV^2.
2. The energy $E_e^{'}$ of the scattered electron must be greater than 14 GeV, corresponding to a fractional electron energy loss in the proton rest-frame of $y = qP/kP \lesssim 0.5$, thus eliminating background from photo-production with a misidentified hadron as an electron at a negligible level (<1%). This cut also suppresses radiative DIS events and hence strongly reduces radiative corrections to the cross section.
3. The angle of the scattered electron must be in the range $160^\circ < \theta_e < 173^\circ$.

Events in the second sub-sample (LAr) must satisfy the following requirements:

1. $Q^2 > 100$ GeV^2.
2. $E_e^{'} > 11$ GeV.
3. $y < 0.7$ to suppress photo-production.
4. $10^\circ < \theta_e < 150^\circ$ to ensure that the electron is contained in the LAr calorimeter and to avoid the transition region between the LAr and BEMC.
5. The quantity $\delta = \sum_{clusters}(E - P_z)$ (with E and P_z being the energy and longitudinal momentum of the calorimetric energy clusters) is required to be within 38 GeV $< \delta <$ 70 GeV. The lower cut excludes effectively photo-production events (<1%), in which the scattered electron is lost down the beam pipe. As does the cut in y discussed above, this cut further reduces radiative corrections to the cross section.

The following additional requirements were imposed on both sub-samples:

1. An event vertex from charged tracks within ± 30 cm around the maximum, z_{mean}, of the vertex distribution; z_{mean} was located at $z = +5$ cm ($+1$ cm) in 1994 (1995).

2. $W^2 > 5000$ GeV^2. This cut ensures enough hadronic activity in the detector and implies a cut on the scaling variable y ($y > 0.055$). The double angle method [15] is used to calculate W^2. This method relies on the angle of the scattered electron and the angle of the four vector sum of all measured hadronic energies. Therefore it is independent of the jet classification.

In both samples Q^2 and y are calculated from the energy and angle of the scattered electron. The final sample contains 112985 events with $Q^2 < 100$ GeV^2 and 5410 (8280) events with 100 GeV$^2 < Q^2 < 4000$ GeV^2 selected from the data taken in 1994 (1995). A fraction of 5% in the low Q^2 sample and of 1% in the high Q^2 sample is compatible with being rapidity gap events.

4 Jet Reconstruction and Recombination Schemes

The analysis bases on a modified JADE jet algorithm [6] as in a previous H1 publication extracting α_s from (2+1) jet rates [1]. At the detector level the modified JADE jet algorithm takes into account the invisible part of the proton remnant r by including a pseudo particle in the clustering procedure representing the missing longitudinal momentum in the event [7]. Performing the JADE algorithm in the laboratary frame two objects i, j with a squared invariant mass m_{ij}^2 are combined to one new object if $y_{ij} = m_{ij}^2/scale^2 < y_c$, where y_c is the resolution parameter. The *scale* is identified with the invariant mass W of the hadronic system X, which is equivalent to the choice of the visible energy for jet reconstruction in e^+e^- reactions. Resulting from studies on the resolution parameter [2, 9] y_c is set to 0.02 as in the first determination of the strong coupling constant at HERA by H1. To combine two objects i and j to a new one k, different recombination schemes (RS) can be used. In the so called Jade RS the new four momentum vector p_k is simply given by $p_k = p_i + p_j$, whereas in the E0 RS ($p_k = (E_i+E_j, (E_i+E_j) * \frac{\vec{p}_i+\vec{p}_j}{|\vec{p}_i+\vec{p}_j|})$) and P RS ($p_k = (|\vec{p}_i + \vec{p}_j|, \vec{p}_i + \vec{p}_j)$) the new four momentum vectors are massless. Hence the resolution criterion is given by $y_{ij} = 2E_iE_j(1 - \cos\theta_{ij})/W^2$, where E_i, E_j denote the energies and θ_{ij} the angle between the two objects i, j, which are under consideration. As long as there are no cuts applied on energy or momentum of the resulting final jets, the Jade and E0 RS are equivalent in the theoretical NLO calculations.

5 The method

In this analysis the fractional (2+1) jet rate in bins of Q^2

$$R_{2+1}(Q^2, y_c) = \frac{\sigma_{2+1}(Q^2, y_c)}{\sigma_{norm}(Q^2, y_c)} = a(Q^2, y_c)\alpha_s(Q^2) + b(Q^2, y_c)\alpha_s^2(Q^2) + \mathcal{O}(\alpha_s^3)$$

is chosen [1, 2] to determine $\alpha_s(\mu_r^2)$ as a function of Q^2, which is here identified with the renormalization scale ($Q^2 = \mu_r^2$). Theoretically R_{2+1} is known to next to leading order, i.e. up to $\mathcal{O}(\alpha_s^2)$ [3]. A expansion of the quotient defining the (2+1) jet rate in terms of α_s determines the coefficients a and b. From this quadratical equation with known theoretical coefficients and measured jet rates the $\alpha_s(Q^2)$ is extracted.

The cross section used as normalization, $\sigma_{norm}(Q^2)$, represents the sum of jet cross sections, where two current jets (σ_{2+1} for (2+1) events) or at least one current jet (σ_{1+1} for (1+1) events) are/is in the final acceptance region. Events with overall more than two current jets are not counted at all. Experimentally R_{2+1} is obtained by N_{2+1}/N_{norm}, with $N_{norm} = N_{2+1} +$

N_{1+1}. Corresponding to σ_{n+1} N_{n+1} is the number of events with n observed current jets in the considered acceptance region neglecting events with more than two reconstructed current jets.

Unfortunately the theoretical $\mathcal{O}(\alpha_s^2)$ calculations are only available in MEPJET [4] and DISENT [5] as Monte Carlo integration programs for the prediction of jet cross sections at the parton level and not as event generators. Therefore the relation between observed jets in the detector and the underlying partonic jet configuration has to be obtained from an available event generator.

The MEPJET Monte Carlo[2] is used in order to compare the measured jet rates and distributions of kinematic variables with the NLO calculation. It is necessary to apply to the NLO Monte Carlo the same phase space restrictions in terms of electron variables and jet quantities as doing in the experimental event selection. The forward direction is the most crucial region for the comparison. The occuring emission of multi-gluon radiation from initial state partons causes a higher reconstructed jet multiplicity. The influence of the multi-gluon radiation increases with decreasing Q^2 because at low Q^2 very low values of the scaling variable $x_B = Q^2/2qP$ are reached. This initial state radiation is naturally not taken into account by a fixed order theory (as in MEPJET). As a consequence the jet rate predicted by the NLO calculations is much smaller than the measured rate without further cuts, particularly at low values of Q^2. Therefore the event generator Monte Carlo is not only used to calculate the correction factors but also to determine cuts necessary to suppress the influence of multi-gluon radiation and hadronization effects. For defining such a phase space region where in principle — except the absolute normalization due to α_s — the NLO prediction is able to describe the data an event generator is highly preferable with a defined parton level comparable to the partonic configuration of the NLO QCD calculation. Hence the final acceptance region for the current jets is chosen using the following criteria for at least one event generator:

- The jet rates in bins of Q^2 predicted by the NLO calculation should be close (in shape and absolute value) to the jet rates predicted by the event generator at the parton level for reasonable values of the QCD parameter $\Lambda^{(4)}_{\overline{MS}}$ as used in MEPJET, e.g. $\Lambda^{(4)}_{\overline{MS}} = 150, 400\,\mathrm{MeV}$.
- The measured (2+1) jet rates should be well described by the event generator model at the detector level.
- Data distributions of other hadronic variables, e.g. jet angles, should be well described by the prediction of the event generator. At partonic level the NLO prediction should be in good agreement with the event generator distributions.

These three requirements can be fulfilled by the use of the event generator LEPTO 6.5 [8]. It has as well a defined parton level very close to the partonic NLO calculation. LEPTO enables event generation using the LO matrix elements alone or by matching leading log parton showers to these matrix elements (MEPS). The parton shower routines base on the Altarelli-Parisi evolution equation and model the multi-gluon radiation. It has been demonstrated that this combination of matrix elements and parton showers gives a good description of the data in a wide range of the phase space [1, 9].

Thereupon in each Q^2 bin a correction factor to the experimental jet rate is calculated by dividing the jet rate obtained from LEPTO 6.5 at the parton level after parton showering by the jet rate at the detector level within the same cuts. In the same way also correction factors from the detector to the hadron level can be determined for the final acceptance region. The possible

[2] In MEPJET the effective number of flavors n_f contributing to the QCD parameter $\Lambda^{(n_f)}_{\overline{MS}}$ (the calculation assumes zero quark masses) is fixed to 5; but in the text presented here always the corresponding $\Lambda^{(4)}_{\overline{MS}}$ will be given.

model dependence introduced by this prescription is included in the systematic error by the use of the event generators HERWIG [26] and ARIADNE [27].

The theoretical predictions are obtained using parton density parametrizations with the factorization scale given by Q^2. The parton densities are usually obtained via evolution from a low lying scale Q_0^2 using a value $\alpha_s(M_Z^2)$ as input parameter, which may differ from that extracted in the analysis presented here. It will be shown, that the error introduced by this inconsistency is small in the kinematic region considered.

6 JADE Jet Analysis

Using the energy clusters in the LAr calorimeter the events were subject to a jet classification applying the modified JADE algorithm as discussed in section 4, where W is calculated as the invariant mass of the four vector sum of all hadronic objects to minimize the influence of the hadronic energy scale uncertainty. A resolution parameter of $y_c = 0.02$ in combination with the $W^2 > 5000$ GeV^2 cut (section 3) ensures an invariant mass squared of the two hard jets > 100 GeV^2 for (2+1)-jet events. After the jet classification a cut in the maximum jet angle ($\theta_{max} = 145°$) was applied in order to ensure that the jets were fully contained in the LAr where the hadronic energy is well measured.

A cut at moderate values of Q^2 ($Q^2 > 40$ GeV^2) avoids phase space regions where the transverse momenta of the hard jets are much larger than Q, but this cut does not suffice to suppress parton showers efficiently. Additional cuts in the jet phase space are necessary. Parton showers produce predominantly jets with small jet angles (θ_{jet}) and small values of

$$z_p = \frac{1}{2}(1 - \cos\theta^*_{jet}) = \frac{E_{jet,i}(1 - \cos\theta_{jet,i})}{\sum_{j=1}^{2} E_{jet,j}(1 - \cos\theta_{jet,j})}$$

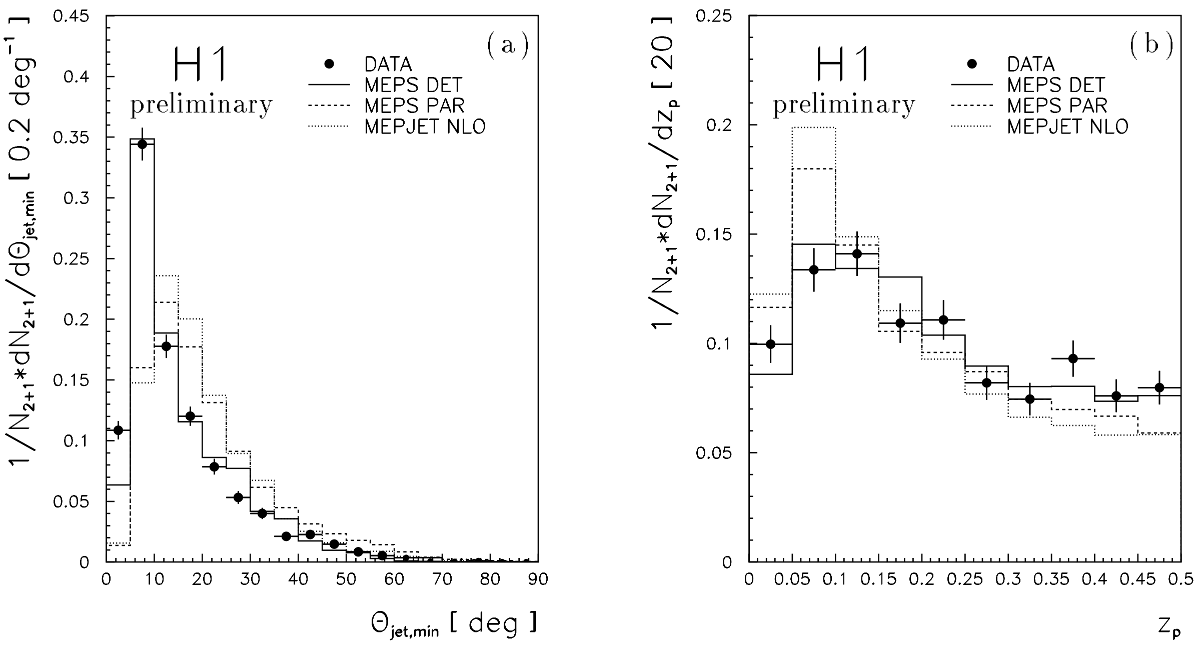

Figure 3: a) The $\theta_{jet,min}$ distribution of the $(2+1)$ jet events for $Q^2 > 40$ GeV^2, $z_p > 0.1$ and $\theta_{max} = 145°$; b) The z_p distribution of the (2+1) jet events for $Q^2 > 40$ GeV^2, $10° < \theta_{jet} < 145°$. The Jade RS is used defining the JADE jets and in both figures the data are represented by the points with statistical error bars only. The solid line represents the prediction of the MEPS model at the detector level and the dashed line the prediction of the same model at the parton level. The MEPJET calculation ($\Lambda^{(4)}_{\overline{MS}} = 230$ MeV) is given by the dotted line. All curves are normalized to the number of events.

where θ^*_{jet} is the smaller of the angles of the two jets in the photon-parton center of mass system ($0 < z_p < 0.5$). θ^*_{jet} is given with respect to the incoming parton direction. Neglecting the masses of the two jets z_p can be determined by the measured energies $E_{jet,j}$ and angles $\theta_{jet,j}$ ($j = 1, 2$) of the jets in the laboratory frame. The jet i corresponds to the jet with the angle θ^*_{jet} in the photon-parton center of mass system. The θ_{jet} and z_p distributions are strongly correlated but account for different tails of the jet phase space in the (θ_{jet}, z_p)-plane. Both are used in this analysis to restrict the jet acceptance region. An optimization according to the criteria given in section 5 results in the cuts $\theta_{jet} > 10°$ and $z_p > 0.1$, in the following refered to the central cut scenario. In this final acceptance region the NLO corrections in the whole accessible range of Q^2 and the Bjorken variable x_B are less than 30%. Due to the finite resolution in m^2_{ij} there are migrations between jet classes at the different levels. For example 57% (69%) of the (2+1) jet events at the detector level are in this class also at the parton level for the BEMC (LAr) sample. The influence of radiative QED corrections on the (2+1) jet rate is less than 5%.

In fig. 3a the distribution of the smallest jet angle ($\theta_{jet,min}$) in a $(2 + 1)$ jet event using the Jade RS is plotted for $Q^2 > 40$ GeV^2 and $z_p > 0.1$. The curves are normalized to the number of events. It is demonstrated that above $\theta_{jet,min} = 5°$ the data is well reproduced

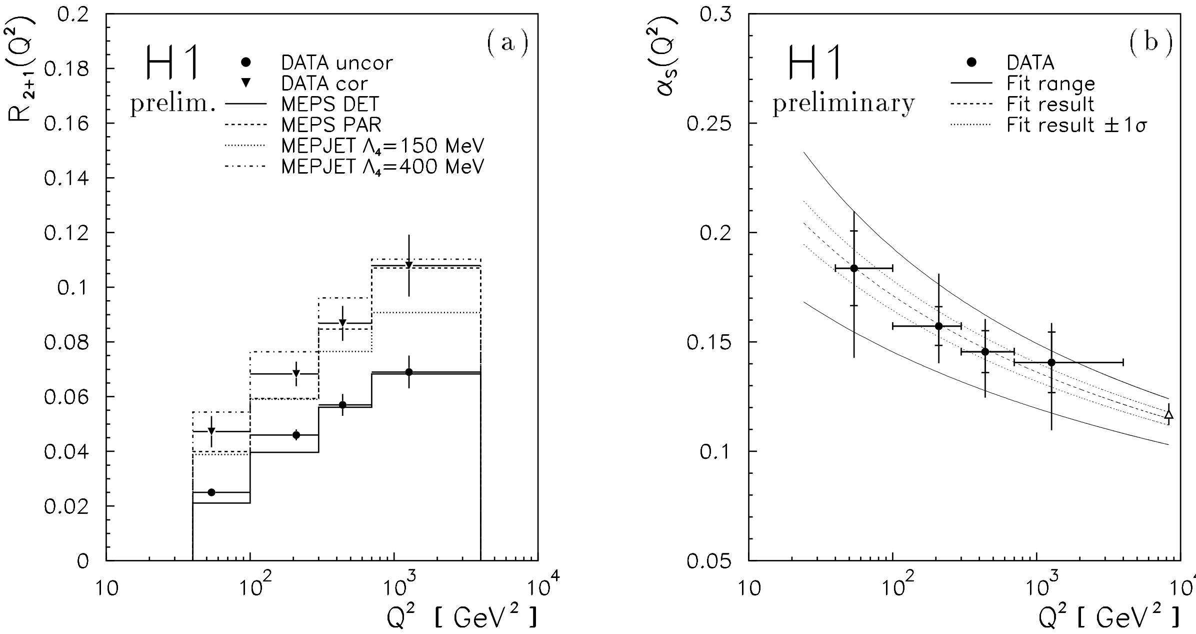

Figure 4: The α_s determination in four bins of Q^2 and at $Q^2 = M_Z^2$ using the JADE jet algorithm in combination with the Jade recombination scheme. The graphs are plotted as functions of Q^2 and the data points are placed at the avaraged Q^2 value in each bin.
a) The measured $R_{2+1}(Q^2)$ (points) and the corrected jet rates $R^{par}_{2+1}(Q^2)$ (triangles) together with the prediction of the MEPS Monte Carlo at the detector level (solid line), parton level (dashed line) and the MEPJET NLO calculations (dotted and dashed dotted lines) for two values of $\Lambda^{(4)}_{\overline{MS}}$ (abbreviated with Λ_4). The rates are determined for $y_c = 0.02$, $Q^2 > 40$ GeV^2, $\theta_{max} = 145°$, $\theta_{jet} > 10°$ and $z_p > 0.1$. The predictions rely on the MRSH parton density parametrization.
b) The α_s values derived from these $R^{par}_{2+1}(Q^2)$ measurements are plotted as points with statistical errors from data and correction factors as inner error bars and total errors as full error bars, see table 3 for numbers. The fit result (dashed line) and the one σ parameter errors (dotted lines) base on the $\alpha_s(Q^2)$ values with their statistical errors only. The solid lines represent the obtained range for $\alpha_s(M_Z^2)$ as determined in this analysis taking into account the systematic uncertainties, see text for details. The open triangle at $Q^2 = M_Z^2$ indicates the world average $\alpha_s(M_Z^2) = 0.118 \pm 0.003$ [18].

Q^2 [GeV^2]	$\langle Q^2 \rangle$ [GeV^2]	R_{2+1} [10^{-3}]	R_{2+1}^{had} [10^{-3}]	R_{2+1}^{par} [10^{-3}]	$f(det \rightarrow had)$	$f(det \rightarrow par)$
40-100	54	$25 \pm 1^{+2}_{-2}$	$33 \pm 4^{+4}_{-3}$	$47 \pm 6^{+4}_{-9}$	$1.32 \pm 0.15 + 0.14$	$1.88 \pm 0.21 - 0.03$
100-300	209	$46 \pm 2^{+3}_{-4}$	$57 \pm 4^{+4}_{-4}$	$68 \pm 5^{+10}_{-5}$	$1.24 \pm 0.05 + 0.06$	$1.48 \pm 0.05 - 0.01$
300-700	440	$57 \pm 4^{+3}_{-0}$	$69 \pm 5^{+4}_{-1}$	$87 \pm 6^{+5}_{-11}$	$1.21 \pm 0.05 + 0.03$	$1.53 \pm 0.06 - 0.07$
700-4000	1272	$69 \pm 6^{+4}_{-1}$	$88 \pm 9^{+6}_{-8}$	$108 \pm 11^{+8}_{-18}$	$1.28 \pm 0.07 - 0.11$	$1.57 \pm 0.08 - 0.23$

Table 1: The (2+1) jet rates (R_{2+1}) with statistical and systematic errors in different bins of Q^2 as measured for the central cut scenario using the Jade RS in the JADE algorithm and corrected to the hadron (R_{2+1}^{had}) and parton level (R_{2+1}^{par}). In addition the correction factors from the detector to the hadron ($f(det \rightarrow had)$) and parton ($f(det \rightarrow par)$) level are included, with errors due to the limited statistics of the Monte Carlo and the model uncertainty (estimated by ARIADNE). The statistical errors on the measured R_{2+1} are given by the data only, whereas the errors on the corrected (2+1) jet rates (R_{2+1}^{had}, R_{2+1}^{par}) include also the statistical errors from the Monte Carlo. The systematic errors on R_{2+1} correspond to the uncertainty on the hadronic energy scale. The systematic errors on R_{2+1}^{had} take into account the energy scale and model uncertainty. For R_{2+1}^{par} in addition the effects of parton showers, hadronization parameters and QCD Monte Carlo models were taken into account similar to the error estimation on α_s as described later on in the text.

by the MEPS model after detector simulation. In addition the MEPS model at the parton level and the MEPJET calculation (with $\Lambda_{\overline{MS}}^{(4)}$ set to 230 MeV) agree reasonably well with each other. Both predict however less $(2+1)$ jet events with smallest $\theta_{jet,min}$ values ($\theta_{jet,min} < 5°$) than measured in the data. A cut in θ_{jet} suppresses parton showers and hadronization effects efficiently. A further improvement in view of the (2+1) jet rates can be reached by a cut in z_p. The z_p distribution is shown (full points) for $Q^2 > 40$ GeV^2 and $\theta_{jet} > 10°$ in fig. 3b.

Using the Jade RS the measured fractional (2+1) jet rate R_{2+1} for $Q^2 > 40$ GeV^2 , $\theta_{jet} > 10°$, $z_p > 0.1$ is shown in fig. 4a by the black points with the statistical error from the data only. The data above $Q^2 = 40$ GeV^2 are divided into four bins containing approximatively equal numbers of (2+1) jet events. The measurements are reasonably well described by the MEPS Monte Carlo at the detector level (full line). In fig. 4a also it can be seen that the jet rate at the parton level in the MEPS model (dashed line) lies between the MEPJET prediction for $\Lambda_{\overline{MS}}^{(4)} = 150$ MeV (dotted line) and $\Lambda_{\overline{MS}}^{(4)} = 400$ MeV (dashed dotted line) as required in section 5.

The correction factors $f(det \rightarrow par)$ for the different Q^2 bins (i.e the ratio between the dashed line and the full line), which are used to calculate the jet rates corrected to the parton level R_{2+1}^{par} (black triangles), are given in table 1. They are of the order 1.5, except for the lowest Q^2 bin. Also the factors $f(det \rightarrow had)$ for correcting the measured rates to the hadron level are included in table 1. It can be seen that hadronization and detector effects lead to lower observable (2+1) jet rates in comparison to the parton level. The given statistical errors on the corrected rates in table 1, the (2+1) jet rates at the hadron R_{2+1}^{had} and the parton level R_{2+1}^{par}, include the statistical error from the data as well as from the calculation of the correction factors. For all calculations the parton density distributions were parametrized using the MRSH [16] results.

The experimental rates corrected to the parton level R_{2+1}^{par} are also plotted in fig. 4a for the standard set of cut parameters (see above) and the Jade RS. They are converted into four values of $\alpha_s(Q^2)$. The results are given in fig. 4b together with the statistical errors from data and correction factors for this particular choice of cut parameters as inner error bars. The extracted values of $\alpha_s(Q^2)$ are fitted [17] to the 2-loop solution of the renormalization group equation taking into account their statistical errors only. The fit, together with its $\pm 1\sigma$ parameter error is also shown in figure 4b. The numerical result at $Q^2 = M_Z^2$ is $\alpha_s(M_Z^2) = 0.115 \pm 0.003\,(stat)$ and the Q^2 dependence of the determined $\alpha_s(Q^2)$ values is very well compatible with the theoretical prediction.

To obtain the systematic uncertainty on $\alpha_s(M_Z^2)$ the fit was repeated for various other fit scenarios changing cuts relevant for the jet analysis. This procedure automatically takes into account the correlation between the four bins in Q^2. See table 2 for a full list of systematic errors covered. Effects due to the uncertainty of the electromagnetic energy scale and the variation of kinematic cuts (see section 3) are negligible.

In order to determine the systematic experimental error the following different kinematic cuts were investigated:

- The cut in z_p was varied between 0.05 and 0.15 for $\theta_{jet} > 5°, 10°, 15°$ leaving the other parameters at their central values. In addition θ_{max} was varied between 140° and 150° leaving the respective other parameters at their central values. The given spreads automatically take into account the correlation of the error sources. The resulting error on $\alpha_s(M_Z^2)$ as determined from the maximum spread of all fit results is $+0.002/-0.003$.
- The hadronic energy scale in the data reconstruction was varied by $\pm 4\%$. The resulting error on $\alpha_s(M_Z^2)$ is $+0.005/-0.003$. Due to the linear dependence of the distances y_{ij} in the jet clustering procedure on the hadronic energy scale it is not necessary to study variations of the resolution parameter y_c as an additional error source.
- The event generator ARIADNE 4.08 [27] was used to study the model dependence, although it does not describe the measured shape of the $R_{2+1}(Q^2)$ distribution. This Monte Carlo model treats the gluon emission in the framework of the colour dipole model as an alternative to the Altarelli-Parisi evolution equation. The resulting fitted $\alpha_s(M_Z^2)$ value using full simulated ARIADNE events was lowered by 0.003.

Source	Variations	$\Delta\alpha_s(M_Z^2)$
Statistics		± 0.003
θ_{jet} and z_p cut	$5°, 8°, 12°, 15° < \theta_{jet} < 145°$ $10° < \theta_{jet} < 140°, 145°, 150°$ $z_p > 0.05, 0.10, 0.15$	${}^{+0.002}_{-0.003}$
Hadronic energy scale	$\pm 4\%$	${}^{+0.005}_{-0.003}$
Model dependence	ARIADNE 4.08	-0.003
Parton density functions	MRSAp-201, GRV92, CTEQ-4pM	± 0.001
Renormalization and factorization scale	$\mu_i^2 = 1/4, 4\,Q^2$ i=f,r	${}^{+0.003}_{-0.007}$
$\Lambda_{\overline{MS}}^{(4)}$ used in the PDF's	0.15 , 0.4 GeV	${}^{+0.003}_{-0.002}$
Parton shower and hadronization parameters	LEPTO 6.5	${}^{+0.004}_{-0.002}$
QCD Monte Carlo model	HERWIG 5.9	-0.007
Recombination schemes	E0 P	$+0.001$ $+0.006$

Table 2: The determination of various systematic uncertainties. The central cut scenario, the MRSH parton density parametrization and the Jade recombination scheme are used as reference.

The final systematic experimental error ($\pm\,0.005$) on $\alpha_s(M_Z^2)$ was taken as the sum of the three given errors in quadrature. The mean value of all fit scenarios coincides with the result of the analysis using the central values of the cuts.

The theoretical uncertainty was investigated by changing various input conditions for the calculations:

- The MRSH parton density function (PDF) used in MEPJET was replaced by the MRSAp-201 [19], GRV92 [20], and the CTEQ-4pM [21] parametrizations. They all use approximately a same $\Lambda^{(4)}_{\overline{MS}}$ value of about 230 MeV. The largest changes observed were ± 0.001.
- The factorization scale μ_f^2 and the renormalization scale μ_r^2 were varied independently between $Q^2/4$ and $4\,Q^2$. The effect on the measured value of $\alpha_s(M_Z^2)$ was $+0.003/-0.007$.
- As a particular point of interest [22, 23] the correlation of the measured value of α_s in this analysis with the value determined while fitting the PDFs was investigated. This was done using the GRV92 PDFs which are available for various $\Lambda^{(4)}_{\overline{MS}}$ values [24] in the range 0.15–0.40 GeV. Although $\alpha_s(M_Z^2)$ used in the PDFs changes by 0.017, the fitted values only differ by $+0.003/-0.002$. This large reduction is due to the fact that the PDFs only depend on α_s via the scaling violations, whereas $R_{2+1}(Q^2)$ is directly proportional to α_s.

A further source of systematic errors stems from the dependence of the correction factors on the Monte Carlo models used to calculate them. These uncertainties were analyzed using the following procedure:

- The LEPTO Monte Carlo uses the JETSET [25] fragmentation model. The fragmentation parameter a of the LUND fragmentation functions was varied between 0.1 and 1, the σ_{pt} parameter and the intrinsic k_T of the struck parton between 440 MeV and 700 MeV. In addition the lower cut-off parameters which control the parton shower generation were varied between 1 and 4 GeV and the lowest value of the invariant mass squared $\hat{s}$ of the two generated partons for which the ME calculations were carried out was changed from 4 GeV^2 to 25 GeV^2. The resulting fitted $\alpha_s(M_Z^2)$ values were in the range 0.119 to 0.113.
- Instead of LEPTO the HERWIG [26] Monte Carlo model with its entirely different treatment of parton showering and hadronization was used to calculate the parton and hadron level. HERWIG is able to describe the shape of the measured $R_{2+1}(Q^2)$ distribution, but not the total normalization. Assuming the correction factors from the detector to the hadron level to be the same as for LEPTO, the fit result for $\alpha_s(M_Z^2)$ was lowered by 0.007.

The total theoretical uncertainty ($+0.006/-0.010$) on $\alpha_s(M_Z^2)$ including the hadronization modeling was taken as the sum of all these errors in quadrature.

The statistical error is the statistical error of the scenario with the central values of the cut parameters (± 0.003). The total systematic uncertainty is taken as the quadratic sum of the systematic experimental and theoretical uncertainties discussed above ($^{+0.008}_{-0.011}$). The result of the analysis using the Jade RS is therefore

$$\alpha_s(M_Z^2) = 0.115 \pm 0.003\,(stat)\,^{+0.008}_{-0.011}\,(sys)\,.$$

The solid lines in figure 4b indicate the full range of $\alpha_s(Q^2)$ obtained in this experiment using the JADE jet algorithm in combination with the Jade RS adding statistical error and systematic uncertainty in quadrature at the scale $Q^2 = M_Z^2$. Hence they correspond to $\alpha_s(M_Z^2) = 0.103$ and 0.124.

	Jade RS				E0 RS	P RS
$\langle Q^2 \rangle$ [GeV^2]	$\alpha_s(Q^2)$	stat	sys	tot	$\alpha_s(Q^2)$	$\alpha_s(Q^2)$
54	0.184	± 0.017	$^{+0.020}_{-0.037}$	$^{+0.026}_{-0.041}$	0.189	0.206
209	0.157	± 0.009	$^{+0.022}_{-0.014}$	$^{+0.024}_{-0.017}$	0.159	0.167
440	0.146	± 0.010	$^{+0.011}_{-0.019}$	$^{+0.015}_{-0.021}$	0.144	0.161
1272	0.141	± 0.014	$^{+0.011}_{-0.028}$	$^{+0.018}_{-0.031}$	0.139	0.141
M_Z^2	0.115	± 0.003	$^{+0.008}_{-0.011}$	$^{+0.009}_{-0.012}$	0.116	0.121

Table 3: The values of $\alpha_s(Q^2)$ together with their statistical, systematic and total uncertainties for the JADE algorithm and the Jade recombination scheme. Also the extracted $\alpha_s(Q^2)$ values using the E0 and P recombination schemes are included.

To obtain the errors on the four measured values of $\alpha_s(Q^2)$ using the Jade RS the following method was applied. Each of the scenarios, except the variation of the factorization and renormalization scale, results in measured values of $\alpha_s(Q^2)$ for the four bins in Q^2. From these values of the different cut scenarios the systematic experimental and theoretical uncertainties at every point are determined in the same way as the uncertainties on $\alpha_s(M_Z^2)$. The total systematic uncertainty using the Jade RS is given by the quadratic sum of these two errors. The outer error bars of the $\alpha_s(Q^2)$ points in figure 4b represent the total uncertainties, which are calculated as the quadratic sum of statistical errors and total systematic uncertainties, see table 3. They correspond well with the full range of $\alpha_s(Q^2)$ given by the $\alpha_s(M_Z^2)$ determined in this analysis using the Jade RS.

To study the dependence of the determined $\alpha_s(M_Z^2)$ value on different recombination schemes the analysis for the central cut scenario was redone using the E0 and P RS instead of the Jade RS. The extracted $\alpha_s(M_Z^2)$ value based on the E0 RS ($\alpha_s(M_Z^2) = 0.116$) is, as expected from a theoretical point of view, very close to the Jade value, whereas for the P RS the fitted value is increased by $+0.006$. This is a consequence of the higher α_s values for the P RS in comparison to the other schemes in all bins of Q^2, except in the highest bin. The values are given in tab. 3. The dependence of the extracted $\alpha_s(M_Z^2)$ value on different recombination schemes is not included in the systematic uncertainty taking the sum in quadrature. The final result of this analysis is therefore

$$\alpha_s(M_Z^2) = 0.115 \pm 0.003\,(stat)\,^{+0.008}_{-0.011}\,(sys)\; + 0.006\,(reco.\ scheme)\,.$$

At large Q^2 the multi-gluon radiation from the initial state partons and hadronization effects are strongly suppressed. Hence the whole analysis was repeated using the Jade scheme in the Q^2 range $150 < Q^2 < 4000$ GeV^2 divided in three bins. This study results in $\alpha_s(M_Z^2) = 0.114 \pm 0.004\,(stat)\,^{+0.008}_{-0.010}\,(sys)\; + 0.005\,(reco.\ scheme)$, which is in excellent agreement with the result of the analysis in the extended Q^2 range presented above.

7 Conclusion

Jet rates in neutral current deep inelastic ep-scattering at HERA are used to extract the strong coupling constant α_s in NLO. The measurement is performed following the strategy developed in [1, 2]. The application of the modified JADE jet algorithm in combination with the Jade recombination scheme leads to the value of $\alpha_s(M_Z^2) = 0.115 \pm 0.003\,(stat)\,^{+0.008}_{-0.011}\,(sys)$.

The systematic error is dominated by the experimental hadronic scale uncertainty and by the theoretical scale dependence and hadronization model dependence. Adding statistical and systematic errors in quadrature yields $\alpha_s(M_Z^2) = 0.115^{+0.009}_{-0.012}$ consistent with the world average $\alpha_s(M_Z^2) = 0.118 \pm 0.003$. A dependence of the extracted $\alpha_s(M_Z^2)$ value on the recombination scheme chosen in the JADE jet algorithm is found. The largest change observed is $+0.006$, which is not included in the systematic uncertainty. Therefore the final result using the JADE jet algorithm is:

$$\alpha_s(M_Z^2) = 0.115 \pm 0.003\,(stat)\,{}^{+0.008}_{-0.011}\,(sys)\; + 0.006\,(reco.\ scheme)\,.$$

This value has to be compared to the combined result of studies of the hadronic final state in the experiments at LEP and SLC [18], which is $\alpha_s(M_Z^2) = 0.122 \pm 0.007$. The error is totally dominated by the theoretical uncertainty associated with same error sources as in the analysis presented in this paper. Analyzing the e^+e^- data the dependence on the used recombination scheme is marginal.

References

[1] H1 Collaboration, T. Ahmed et al., Phys. Lett. **B346** (1995) 415.

[2] R. Nisius, PhD thesis, Aachen preprint PITHA 94/21 (1994).

[3] D. Graudenz, Phys. Lett. **B256** (1991) 518; D. Graudenz, Phys. Rev. **D49** (1994) 3291; J.G. Körner, E. Mirkes and G.A. Schuler, Int. J. Mod. Physics **A4** (1989) 1781; T. Brodkorb and J.G. Körner, Z. Phys. **C54** (1992) 519.

[4] E. Mirkes and D. Zeppenfeld, Phys. Lett. **B380** (1996) 105.

[5] M. Seymour and S. Catani, CERN-TH 96-29.

[6] JADE Collaboration, W. Bartel et al., Z. Phys. **C33** (1986) 23.

[7] D. Graudenz and N. Magnussen, Proc. Workshop ‘Physics at HERA’, DESY, Hamburg, Vol. 1 (1991) 261, and references therein.

[8] G. Ingelman, LEPTO version 6.5, unpublished program manual; see also: LEPTO 6.1, Proc. Workshop ‘Physics at HERA’, DESY, Hamburg, Vol. 3 (1991) 1366.

[9] H1 Collaboration, I. Abt et al., Z. Phys. **C61** (1994) 59.

[10] H1 Collaboration, I. Abt et al., Nucl. Instr. and Meth. **A386** (1997) 310-347 and Nucl. Instr. and Meth. **A386** (1997) 348-396.

[11] H1 Calorimeter Group, B. Andrieu et al., Nucl. Instr. Meth. **A336** (1993) 460.

[12] H1 Calorimeter Group, B. Andrieu et al., Nucl. Instr. Meth. **A350** (1994) 57.

[13] H1 Collaboration, S. Aid et al., Nucl. Phys. **B439** (1995) 471.

[14] H1 Calorimeter Group, B. Andrieu et al., Nucl. Instr. Meth. **A336** (1993) 499.

[15] S. Bentvelsen et al., Proc. Workshop ‘Physics at HERA’, DESY, Hamburg, Vol. 1 (1991) 23; K.C. Hoeger, ibid., Vol. 1, 43.

[16] A.D. Martin, W.J. Stirling and R.G. Roberts, Proc. of the Workshop on Quantum Field theory and Theoretical Aspects of High Energy Physics, eds. B. Geyer and E.M. Ilgenfritz, 11 (1993), Durham, DTP 93-86, and Rutherford, RAL 93-077.

[17] F. James and M. Ross, MINUIT program manual (version 94.1), CERN Program Library.

[18] Particle Data Group, R.M. Barnett et al., Phys. Rev. **D54** (1996) 1.

[19] A.D. Martin, R.G. Roberts and W.J. Stirling, Phys. Lett. **B356** (1995) 89.

[20] M. Glück, E. Reya and A. Vogt, Z. Phys. **C53** (1992) 127.

[21] CTEQ Collaboration, H.L. Lai et al., Michigan State Univ., MSU-HEP-41024 (1994).

[22] B.R. Webber, Proceedings of ICHEP in Glasgow, 20-27 July 1994, Vol. 1, 213.

[23] J. Chyla and J. Rames, Proceedings of the workshop "Future Physics at HERA" at DESY, Hamburg 1996, Vol. 1, 529-532.

[24] A. Vogt, Phys. Lett. **B354** (1995) 145.

[25] T. Sjöstrand, PYTHIA 5.7 and JETSET 7.4, physics and manual, CERN-TH 7112-93.

[26] B.R. Webber, HERWIG version 5.9, unpublished program manual; see also: HERWIG 5.4, Proc. Workshop 'Physics at HERA', DESY, Hamburg, Vol. 3 (1991) 1354.

[27] L. Lönnblad, ARIADNE version 4.08, Comput. Phys. Commun. **71** (1992) 15, and references therein.